

MDPI

Article

# Microstructure and Properties of Semi-Solid 7075 Aluminum Alloy Processed with an Enclosed Cooling Slope Channel

Zhaoqiang Li <sup>1</sup>, Yongkun Li <sup>1,2,\*</sup>, Rongfeng Zhou <sup>1,2,\*</sup>, Lingzhi Xie <sup>1</sup>, Qiansi Wang <sup>1</sup>, Lingzhi Zhang <sup>1</sup>, Qiang Ji <sup>1,3</sup> and Bin Xu <sup>1,3</sup>

- Faculty of Material Science and Engineering, Kunming University of Science and Technology, Kunming 650093, China; xubinyyy@126.com (B.X.)
- <sup>2</sup> City College, Kunming University of Science and Technology, Kunming 650093, China
- <sup>3</sup> Chengdu Tonglin Casting Industrial Co., Ltd., Chengdu 610000, China
- \* Correspondence: liyongkun@kust.edu.cn (Y.L.); zhourfchina@hotmail.com (R.Z.)

**Abstract:** In this study, an enclosed cooling slope channel (ECSC) was used to produce a semi-solid slurry of the 7075 aluminum alloy. The effects of the pouring temperature and the rate of cooling water on the microstructure of the semi-solid slurry were studied. The microstructure, solidification behavior, mechanical properties, and fracture mechanism of rheological squeeze casting (Rheo-SC) and liquid squeeze casting (LSC) samples were compared. The results indicate that lowering the pouring temperature and increasing the rate of cooling water can refine the crystals of the semi-solid slurry. The best process is a pouring temperature of 670 °C and a rate of cooling water of 200 L/h. The microstructure of the LSC samples was made up of coarse dendritic crystals, but the microstructure of the Rheo-SC samples was made up of almost spherical primary  $\alpha_1$ -Al and refined secondary  $\alpha_2$ -Al under this method. The ultimate tensile strength, yield strength, and elongation of the Rheo-SC samples were 238 MPa, 151 MPa, and 5.2%, respectively, which were 10%, 10.5%, and 44.4% higher than those of the LSC sample. The key factor contributing to the increased performance of the Rheo-SC samples is the combination of decreased casting flaws, strengthened grain refinement, and improved segregation.

**Keywords:** 7075 aluminum alloy; semi-solid slurry; rheological squeeze casting; microstructure; mechanical properties



Citation: Li, Z.; Li, Y.; Zhou, R.; Xie, L.; Wang, Q.; Zhang, L.; Ji, Q.; Xu, B. Microstructure and Properties of Semi-Solid 7075 Aluminum Alloy Processed with an Enclosed Cooling Slope Channel. Crystals 2023, 13, 1102. https://doi.org/10.3390/cryst13071102

Academic Editor: José L. García

Received: 8 June 2023 Revised: 7 July 2023 Accepted: 12 July 2023 Published: 14 July 2023



Copyright: © 2023 by the authors. Licensee MDPI, Basel, Switzerland. This article is an open access article distributed under the terms and conditions of the Creative Commons Attribution (CC BY) license (https://creativecommons.org/licenses/by/4.0/).

## 1. Introduction

Al–Zn–Mg–Cu alloys are frequently employed in the aerospace and automotive industries due to their high specific strength and low density [1–3]. The conventional casting method, which is regarded as being unsuitable for casting, makes it easy for defects, like hot cracking, porosity, and shrinkage cavities to occur because of the high level of Al–Zn–Mg–Cu alloying. Currently, Al–Zn–Mg–Cu alloy components are primarily manufactured using forging, rolling, extrusion, and other plastic processing methods. However, these procedures are costly, and it is difficult to fabricate parts with complicated shapes, which severely restricts the range of applications for Al–Zn–Mg–Cu alloys [4–6].

Squeeze casting is a highly efficient and environmentally friendly near-net forming technology that applies pressure to the molten alloy inside the mold so that the melt can be filled and solidified under pressure [7]. However, conventional squeeze casting products have a series of problems, such as shrinkage, porosity, and coarse dendrites in the microstructure. Rheological squeeze casting (Rheo-SC) uses a semi-solid slurry with a certain fraction solid, which can flow smoothly during the filling process and has a small solidification shrinkage, which helps to avoid shrinkage and porosity and reduce defects such as hot cracking. The materials produced by rheological squeeze casting are characterized by high density, low defects, and excellent mechanical properties [8–11].

Crystals 2023, 13, 1102 2 of 15

Al-Zn-Mg-Cu alloy components with complex shapes and great performance can be produced using Rheo-SC. The semi-solid slurry production and squeeze casting are two steps that make up the Rheo-SC process; creating a high-quality semi-solid slurry is essential to produce components with better mechanical properties [12]. A number of researchers have been studying the way to prepare semi-solid slurries in recent years. For example, LIU et al. produced an Al-8 Si-0.5 Fe alloy semi-solid slurry by vibrating a sloping plate and then combined that with die-casting to develop castings with good mechanical and thermal conductivity [13]. Large thin-walled parts of the Al–Zn–Mg–Cu alloy were prepared by QI et al. using an air-cooled stirring rod rheological die-casting technique supported by ultrasonic vibration, and research on the microstructure and corrosion resistance of the parts was conducted [14]. By changing the pneumatic pressure to oscillate the melt flow, GAO et al. generated a semi-solid slurry of the A356 alloy and then utilized numerical simulations for analyzing the melt flow rate and temperature field during the formulation of semi-solid slurries. According to the results, the oscillating melt flow altered the solute distribution and substantially decreased the grain size [15]. ZHOU et al. studied the planetary stirring process parameters affecting the semi-solid slurry quality of the A356 alloy. The findings verified that the melt flow effect favors the development of spherical crystals and that strong shear and turbulent flow effects encourage grain nucleation and uniform growth. An oscillation at 20 Hz for three minutes had the best effect on the refinement of the melt, the average grain diameter was  $50 \mu m$ , and the mechanical properties of the casting were also improved [16]. Jahanbakhshi et al. used a cooling slope during the solidification of the A356 alloy while introducing mechanical vibration to the melt to refine the grains [17]. The rheological forming of aluminum alloys has been the subject of numerous studies, but little is known about the process when it comes to the Al–Zn–Mg–Cu alloy, particularly when it comes to the integration of the slurry preparation and forming processes.

The Al–Zn–Mg–Cu alloy is a typical heat treatment-strengthened alloy, which can only be heat treated to obtain excellent overall properties to meet service performance requirements. However, this article only discusses the properties of Al–Zn–Mg–Cu alloy semi-solid slurry preparation and rheological forming castings to provide quality castings that must be heat treated at a later stage. In this paper, a bottom injection squeeze casting machine was used in conjunction with an independently created and designed enclosed cooling slope channel (ESCS) [18] to produce a semi-solid slurry of the 7075 aluminum alloy to make thin-walled bushing parts. The impact of two variables—the pouring temperature and the rate of cooling water—on the development of the microstructure of the semi-solid slurry of the 7075 aluminum alloy was carefully examined. The Rheo-SC and liquid squeeze casting (LSC) samples' microstructure, solidification behavior, mechanical properties, and fracture mechanisms were also explored.

### 2. Experimental Procedure

#### 2.1. Material

The basic material for this study was a commercial 7075 aluminum alloy, and the chemical composition (measured in weight percentages) was 5.45% Zn, 2.17% Mg, 1.26% Cu, 0.12% Si, 0.15% Fe, 0.04% Mn, and Al balanced. The alloy's solidus and liquidus temperatures, which were discovered using differential scanning calorimetry (DSC) at a heating rate of 10 °C/min, are 584 °C and 643 °C, respectively, and the eutectic phase melting point is 477 °C. The DSC curve is shown in Figure 1a, and the fraction solid of the 7075 alloy at different temperatures calculated from the DSC curve is shown in Figure 1b [19].

Crystals **2023**, 13, 1102 3 of 15

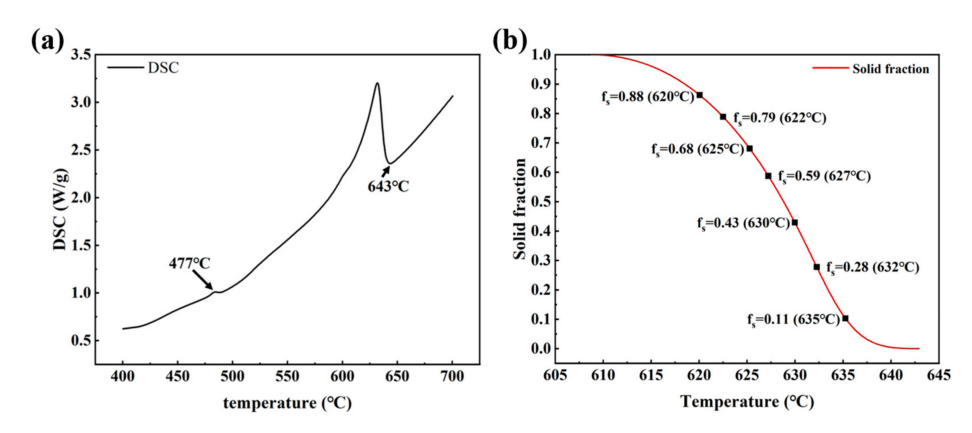
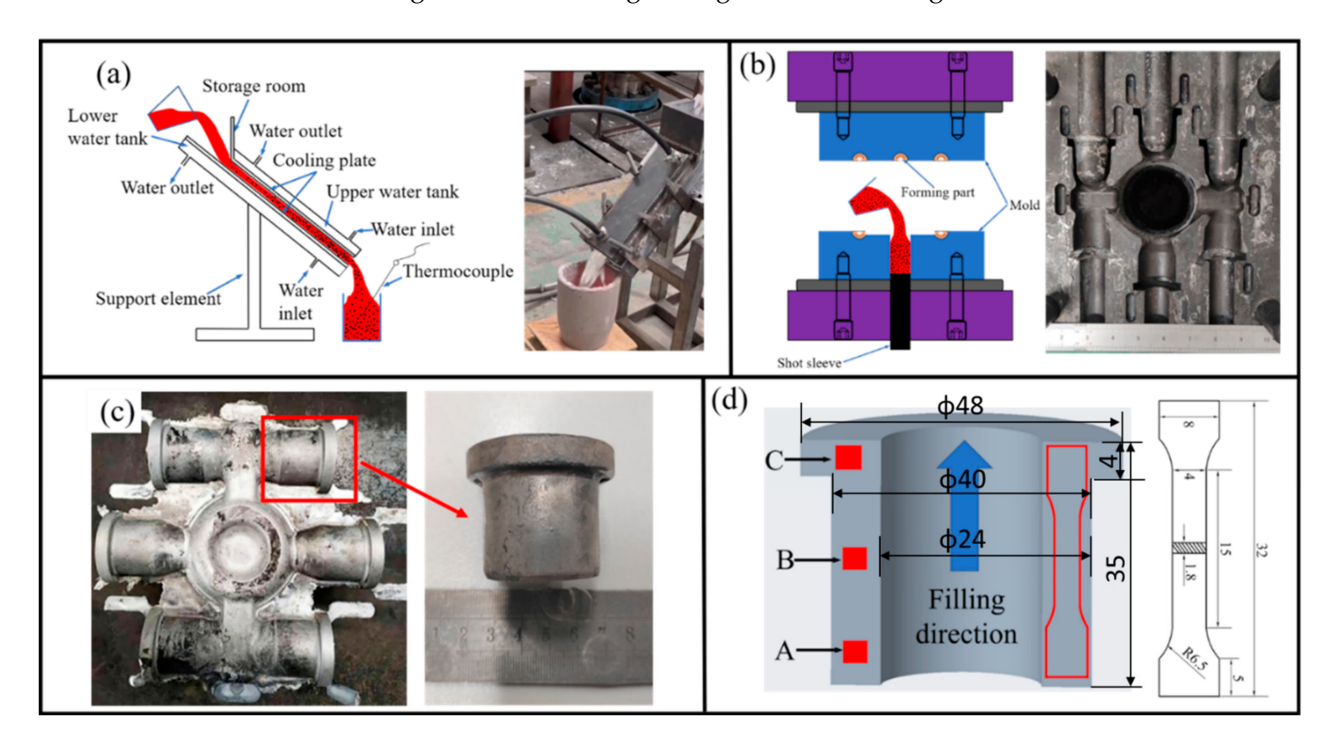


Figure 1. (a) DSC curve; (b) Fraction solid of 7075 alloy.

# 2.2. Production of Semi-Solid Slurry and Rheo-SC

Figure 2a shows the production of a semi-solid slurry. First, about 2 kg of alloy ingots were first heated to 750 °C by an intermediate frequency induction furnace. C<sub>2</sub>Cl<sub>6</sub> powders, which made up 0.5% of the melt weight, were then added for degassing and were allowed to stand for 10 min. When the melt reached the predetermined pouring temperature, it was poured into the ECSC to generate a semi-solid slurry. The melt's temperature was detected using a K-type thermocouple. The channel length of the ECSC was 300 mm, the height was 5 mm, and the inclination angle was 45°. At the channel's outlet, a copper container that was water-cooled was used to collect the semi-solid slurry. To investigate the fraction solid of the slurry, the temperature of the slurry was measured once it had been collected. To obtain its microstructure, the semi-solid slurry was then quickly quenched in water. As shown in Figure 2b, the semi-solid slurry for Rheo-SC is instead transferred to the bottom barrel of the injection squeeze casting process using a preheated graphite crucible. In the Rheo-SC process, the injection punch moves at a speed of 21 mm/s, the die is preheated to 300 °C, the forming pressure is 90 MPa, and the holding pressure is maintained for 15 s. At the same time, the LSC parts were also prepared using the above process parameters; the resulting thin-wall bushing castings are shown in Figure 2c.



**Figure 2.** (a) Slurry preparation process; (b) Diagram of the squeeze casting process and mold; (c) Thin-wall bushing casting; (d) Diagram of metallographic and tensile samples sampling location.

Crystals **2023**, 13, 1102 4 of 15

#### 2.3. Microstructure Analysis and Tensile Test

The center of the water-quenching block is where the microstructure of the slurry is found. The casting's metallographic and tensile samples were cut in accordance with the locations illustrated in Figure 2d. Following rough grinding, fine grinding, and polishing, the metallographic samples were etched with Keller reagent. Using scanning electron microscopy with quantitative energy dispersive X-ray spectroscopy (SEM, Nova Nano SEM 450, FEI, Hillsboro, OR, USA), as well as optical microscopy (OM, Leica, Buffalo Grove, IL, USA), the microstructure of the semi-solid slurry and casting samples was examined. The distribution and size of the grains in the Rheo-SC and LSC samples were investigated using electron back-scattered diffraction (EBSD, NordlysNano, Oxford, UK). To ascertain the phase composition of the casting samples, X-ray diffraction (XRD, Empyrean, Malvern PANalytical, Almelo, Netherlands) was utilized. The image analysis software Image Pro Plus 6.0 was used to calculate the average grain diameter (D =  $(4A/\pi)^{1/2}$ , A is the grain area) and the shape factor (F =  $(4A\pi)/P^2$ , P is the grain circumference) [20] of the grains. The tensile test was conducted using a universal testing device (AG-X plus 100KN, Japan) in accordance with the GB/T 228.1-2010 standard, and the final tensile property index was determined by averaging the measurement results of three tensile samples.

#### 3. Results and Discussion

# 3.1. Effect of Pouring Temperature on Slurry's Semi-Solid Microstructure

Table 1 lists the different parameters of the microstructure of the semi-solid slurries using various techniques. The microstructure of the semi-solid slurry of the 7075 alloys can be seen in Figure 3 at various pouring temperatures, and the rate of the cooling water was 200 L/h. According to Figure 3, the semi-solid slurry's microstructure is primarily subspherical and rosette-like, with a tiny proportion of slightly coarse petal-like grains and damaged dendrites. According to the circle position in Figure 3c, as the pouring temperature increases, the microstructure becomes coarser, the roundness of the grains declines, and some grains maintain a dendritic shape. This partially reduces the homogeneity of the slurry' microstructure and is unfavorable for the ensuing forming process.

**Table 1.** Characteristic parameters of the microstructure of semi-solid slurries under different casting processes.

No.	Pouring Temperature (°C)	Rate of Cooling Water (L/h)	Outlet Temperature (°C)	Average Grain Diameter (μm)	Average Shape Factor
1	660	200	627	$34\pm14$	$0.71 \pm 0.16$
2	670	200	629	$35 \pm 17$	$0.67 \pm 0.18$
3	680	200	634	$41\pm15$	$0.61\pm0.20$
4	670	100	631	$42\pm23$	$0.56\pm0.21$
5	670	300	625	$36 \pm 19$	$0.64 \pm 0.19$

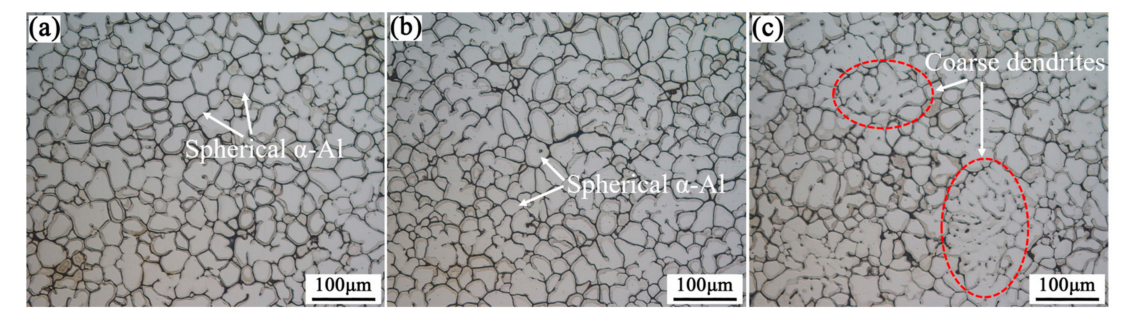


**Figure 3.** Microstructure of semi-solid slurry at different pouring temperatures: (a) 660; (b) 670; (c) 680.

Crystals 2023, 13, 1102 5 of 15

The ECSC is where the primary  $\alpha$ -Al forms crystals in the slurry. Figure 4 depicts a schematic diagram of grain production at various periods of slurry preparation. When the superheated alloy melt is poured into the channel at the beginning of the pouring procedure, the dual action of the channel surface and cooling water causes the melting heat in contact with the channel surface to be rapidly lost and cooled to below the liquid phase line temperature. Most of the primary  $\alpha$ -Al crystals will drain out with the melt due to melt flow inertia, but a tiny amount will stick to the inner channel walls and create a residual solidification shell [21]. The temperature and concentration gradients inside the melt have a substantial impact on nucleation in the early period of pouring. Some of the grains grow in a dendritic pattern as a result of the inhomogeneity of the temperature and concentration fields. In comparison, others are remelted at high temperatures when they do not reach the essential nucleation radius [22]. As seen in Figure 4a, some of the dendrites can also be seen in the microstructure images.

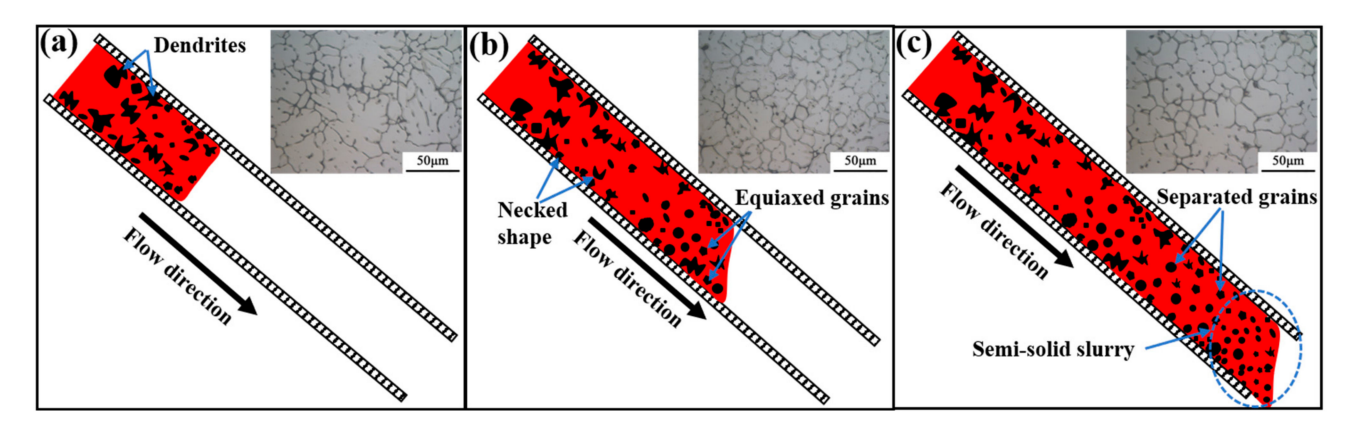


**Figure 4.** Evolution of primary  $\alpha$ -Al in semi-solid slurries at different periods of pouring: (a) Early period; (b) Middle period; (c) Final period.

During the middle period of pouring, the melt continuously descends due to gravity, changing its density, temperature, and solute concentration. Some of the dendrites' necks and fragments separate as a result of convection and melt solute enrichment. The amount of primary  $\alpha$ -Al crystals increases as the dendritic fragments progressively develop into free grains. The microstructure photographs of the slurry, as shown in Figure 4b, reveal an increase in the number of grains and a propensity for the shape to become more spherical and equiaxed.

The initial grains formed on the surface of the cooling channel at the end of the pouring process (Figure 4c) separate from the channel surface as a result of the vigorous scouring and shearing caused by the flow inertia of the melt, as the cooling plate surface chilling effect results in a significant amount of explosive nucleation of the melt. As a result, new nucleation and continuous separation are continuously encouraged by the cooling channel's free surface, increasing the amount of primary  $\alpha$ -Al [23–25]. At the same time, the relatively uniform temperature, solute, and concentration fields within the melt inhibit the anisotropic growth of the nuclei, resulting in a uniform production rate in all directions of the nuclei. In addition, the increase in the number of nuclei, which creates competition during growth, also inhibits the anisotropic growth of nuclei. Under the combined effect of these factors, the nuclei eventually grow into equiaxed, spherical, or rose-shaped crystals.

The temperature field and velocity field on the channel surface both play a role in the creation of the primary  $\alpha$ -Al. The relationship between the thickness of the velocity boundary layer ( $\delta$ ) and the thickness of the temperature boundary layer ( $\delta_t$ ) on the cooling channel surface is shown in the following equation [26]:

$$\delta_t = \frac{\delta}{Pr^{1/3}}$$

Crystals 2023, 13, 1102 6 of 15

The Prandtl number of liquid metal, Pr, is 0.004–0.029. As a result, the  $\delta_t$  is significantly bigger than the  $\delta$ . While the temperature boundary layers are dispersed throughout almost the entire melt, there are only very small velocity boundary layers on the surface of the cooling channels, which promotes uniform melt nucleation.

The pouring temperature is a key factor in the nucleation and development of primary  $\alpha$ -Al during the formation of the semi-solid slurry. The following equation can be used to express the alloy melt's nucleation rate [27]:

$$N_s = A_s exp\left[-\frac{\Delta G_A}{kT}\right] exp\left[-\frac{\alpha\sigma^3 T_m^2}{\left(L_m \Delta T\right)^2} \cdot \frac{2 - \cos\theta + 3\cos\cos^2\theta}{4}\right]$$

where  $A_s$  is a constant,  $\Delta G_A$  is the diffusion activation energy, k is the Boltzmann constant, T is the thermodynamic temperature,  $\alpha$  is the shape factor of the crystals (spherical nucleus:  $\alpha = 16\pi/3$ ),  $\sigma$  is the solid/liquid interface energy,  $L_m$  is the latent heat,  $\Delta T$  is the degree of melt undercooling, and  $\theta$  is the wetting angle. As can be seen from the equation above, the degree of melt undercooling decreases as the pouring temperature increases, and the chilling action on the surface of the cooling channel weakens, which lowers the rate at which the primary  $\alpha$ -Al crystallizes. The amount of primary  $\alpha$ -Al may also be decreased by higher pouring temperatures because they may remelt the already produced nuclei. According to Figure 3c, the slurry microstructure started displaying coarse dendritic crystals as the pouring temperature increased from 660 °C to 680 °C. When entering the slurry collection crucible at a high casting temperature, the slurry's properties of high temperature and low viscosity make it easier for it to collide with the wall of the crucible, creating turbulence and air involvement that impairs the performance of subsequent forming components.

The relative frequency distribution of the grain size at each pouring temperature is shown in Figure 5 along with the change in the average grain diameter and shape factor of the slurry' microstructure with the casting temperature. According to Figure 5a, the average grain diameter of the grains increases from (34  $\pm$  14)  $\mu m$  to (41  $\pm$  15)  $\mu m$  when the casting temperature rises from 660 °C to 680 °C, while the shape factor decreases from (0.71  $\pm$  0.16) to (0.61  $\pm$  0.2), making the grains coarser and less rounded. It is clear that lowering the pouring temperature would help obtain fine spherical grains. If the pouring temperature is too low, the slurry will fill the channel and reduce the effectiveness of the slurry preparation while also wasting material because of the high melt viscosity that would result. In addition, if the casting temperature is too low, the slurry will solidify into a shell, and the cooling effect of the ECSC will not be fully utilized when the high-temperature alloy liquid flows through the solidified shell layer, which will affect the impact of refining the slurry microstructure and is not conducive to the subsequent forming of complex parts. Therefore, considering the slurry preparation efficiency and slurry quality, the optimum pouring temperature is considered to be 670 °C.

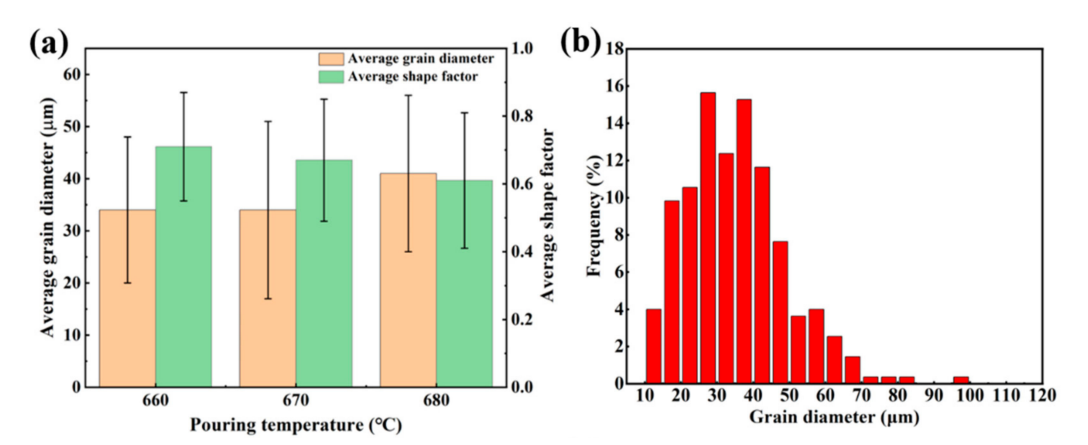
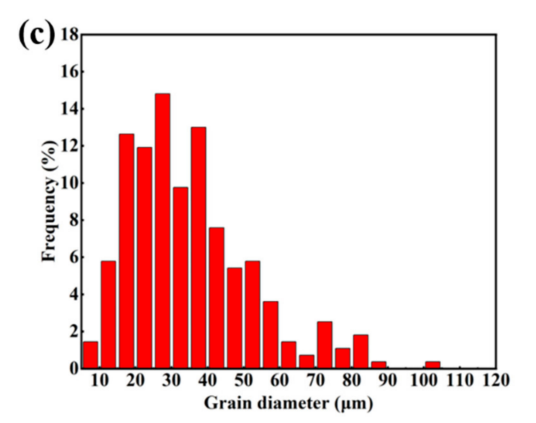
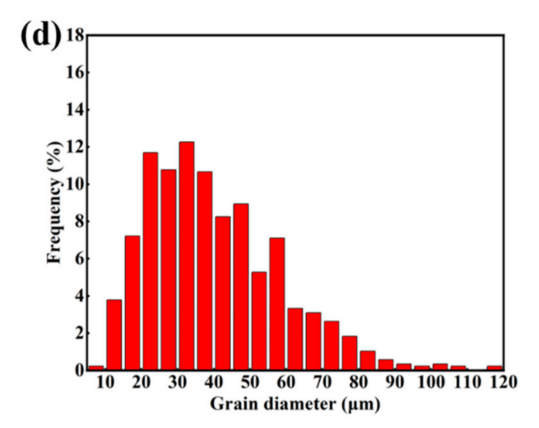


Figure 5. Cont.

Crystals 2023, 13, 1102 7 of 15





**Figure 5.** (a) The effects of pouring temperature on average grain diameter and shape factor; Relative frequency distribution of grain size at each pouring temperature: (b)  $660 \,^{\circ}$ C; (c)  $670 \,^{\circ}$ C; (d)  $680 \,^{\circ}$ C.

## 3.2. Effect of Rate of Cooling Water on Slurry's Semi-Solid Microstructure

The microstructure of the slurry with different rates of cooling water and a pouring temperature of 670 °C can be seen in Figure 6. When the rate of cooling water is 100 L/h, the cooling effect of the ECSC channel to the alloy liquid is weak, and the heat taken away from the melt in unit time is less, which is not enough to provide subcooling conditions for the formation of a large number of free crystals at the early stage of solidification, so the metallographic photographs at this time show that the grain composition of the semi-solid slurry is not well-developed equiaxed dendritic grains. According to Figure 6a, the primary  $\alpha$ -Al grains had an average grain diameter of (42  $\pm$  23)  $\mu m$  and a shape factor of 0.56  $\pm$  0.21. As the chilling effect on the melt increases, the quantity of grains increases, and the grains become finer and circular when the rate of cooling water increases to 200 L/h. As seen in Figure 6b, at this point, the shape factor increases to 0.67, and the average grain diameter decreases to 35  $\mu m$ . The microstructure of the slurry does not prominently modify as the rate of cooling water is further increased to 300 L/h, although the average grain diameter of the grains does slightly increase, as seen in Figure 6c.

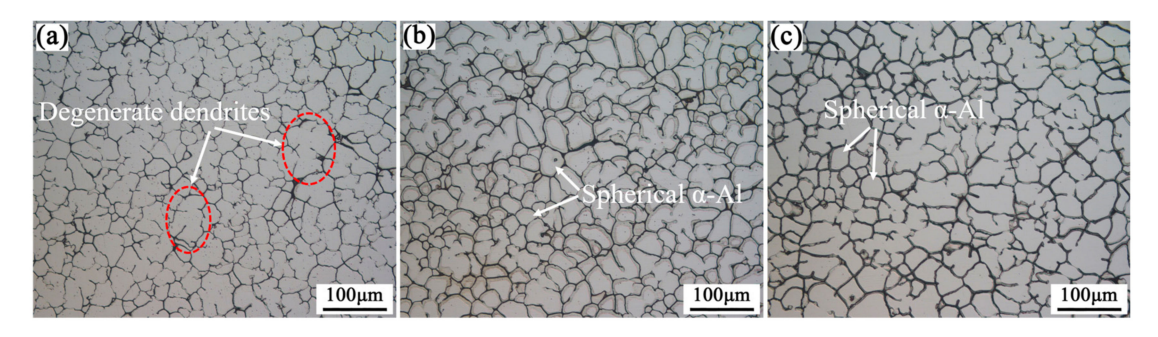


**Figure 6.** Microstructure of semi-solid slurry of 7075 alloys at different rates of cooling water: **(a)** 100 L/h; **(b)** 200 L/h; **(c)** 300 L/h.

The flow velocity of the rate of cooling water has a significant impact on the melt's cooling rate, which in turn influences the melt's nucleation rate. The following equation can be used to explain how the cooling rate affects the melt nucleation rate [28]:

$$N_c = 10^{c_0 - m \cdot Ig[\frac{2 - 3\cos\theta + \cos^2\theta}{4}]} \cdot \frac{R_c}{S_v V}$$

where  $c_0$  is a constant, m is the material regression coefficient ( $m_{\rm Al} = 0.54$ ),  $\theta$  is the wetting angle,  $R_c$  is the cooling rate,  $S_v$  is the effective heterogeneous core surface area, and V is the melt volume. A higher melt nucleation rate is produced by a quicker melt cooling rate, which is accelerated by a higher rate of cooling water. The primary  $\alpha$ -Al's ability to develop

Crystals 2023, 13, 1102 8 of 15

dendritically was limited by the greater cooling rate, which also reduced solute transport. However, at a quick cooling rate, primary  $\alpha$ -Al nuclei frequently develop into dendrites, which degrades the quality of the slurry.

The relative frequency distribution of the grain size at each rate of cooling water can be seen in Figure 7, along with the change in the average grain diameter and shape factor of the slurry microstructure with the rate of cooling water. It has been discovered that increasing the rate of cooling water can produce a fine, rounded semi-solid slurry microstructure by causing the primary  $\alpha$ -Al grain size to first decrease and then slightly increase, as well as causing the shape factor to increase and then slightly decrease. However, the characteristic parameters of the slurry microstructure appear to change irregularly when the rate of cooling water increases above 200 L/h, and continuing to increase the rate of cooling water has little impact on the slurry microstructure, so the rate of cooling water for the ECSC process should be kept at 200 L/h.

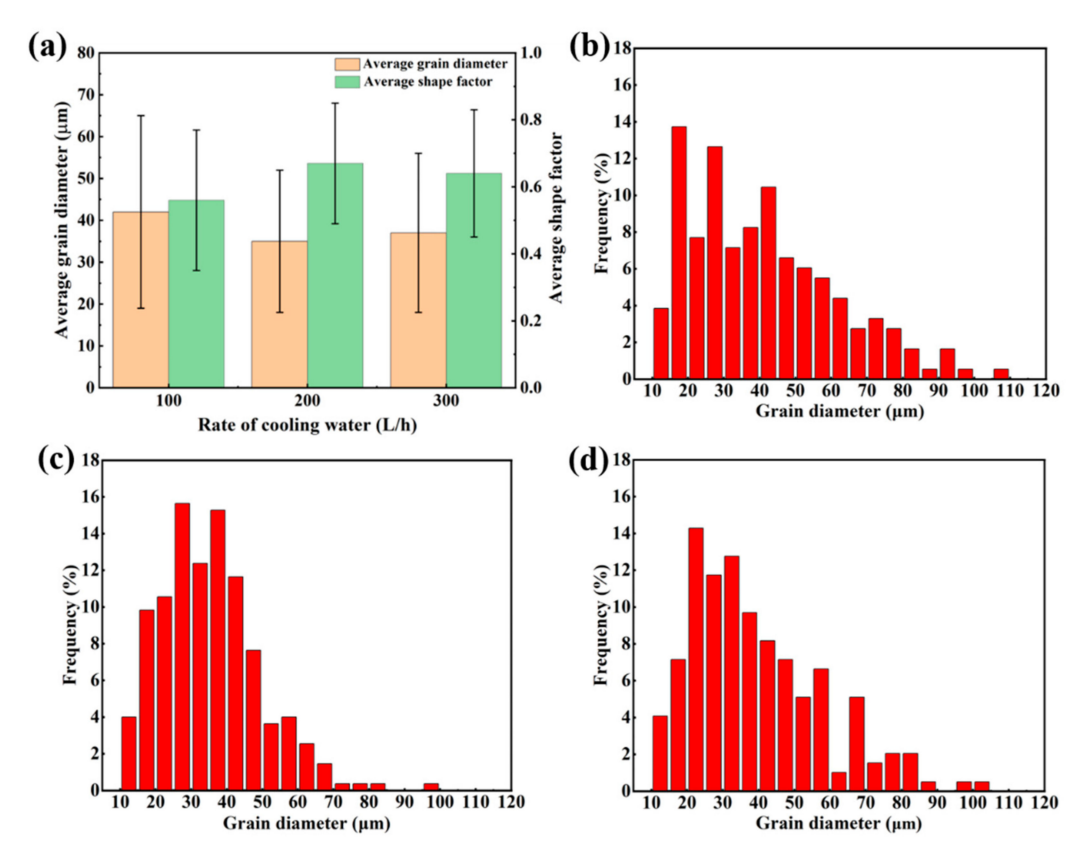


**Figure 7.** (a) The effects of the rate of cooling water on average grain diameter and shape factor; Relative frequency distribution of the grain size at each rate of cooling water: (b) 100 L/h; (c) 200 L/h; (d) 300 L/h.

## 3.3. Microstructure and Mechanical Properties of Casting

#### 3.3.1. Microstructure

The microstructure of the LSC and Rheo-SC samples can be seen in Figure 8. According to Figure 8, the LSC samples are primarily made up of coarse dendrites, some of which have grains larger than 200  $\mu$ m, and numerous fine diffuse secondary  $\alpha_2$ -Al particles created by the liquid phase that was left in the melt and scattered between the primary  $\alpha$ -Al. Due to the die temperature (300 °C) being much lower than the melt temperature during the LSC process, there is a significant temperature gradient when the melt is poured into the die. This causes a rapid loss of heat from the melt, followed by the formation of a solidified shell layer with some shrinkage, which causes a barrier to form between the die and the melt, degrading the pertinent contact conditions and impairing the subsequent heat transfer [29]. Additionally, during LSC, substantial intergranular eutectic phase segregation is typically

*Crystals* **2023**, *13*, *1102* 9 of *15* 

caused by the high casting temperature and quick solidification [30], as shown in the dark positions in Figure 8a,c,e. As can be seen in Figure 8, the dendrite arms at positions B and C of the LSC part are coarser and contain more intergranular eutectic phase segregation than position A. This is because position A is closest to the sprue, and the cooling rate at C is faster compared to position A, resulting in a much faster solidification rate than position A. As a result, the casting's filling direction causes an increase in the segregation of the intergranular eutectic phase.

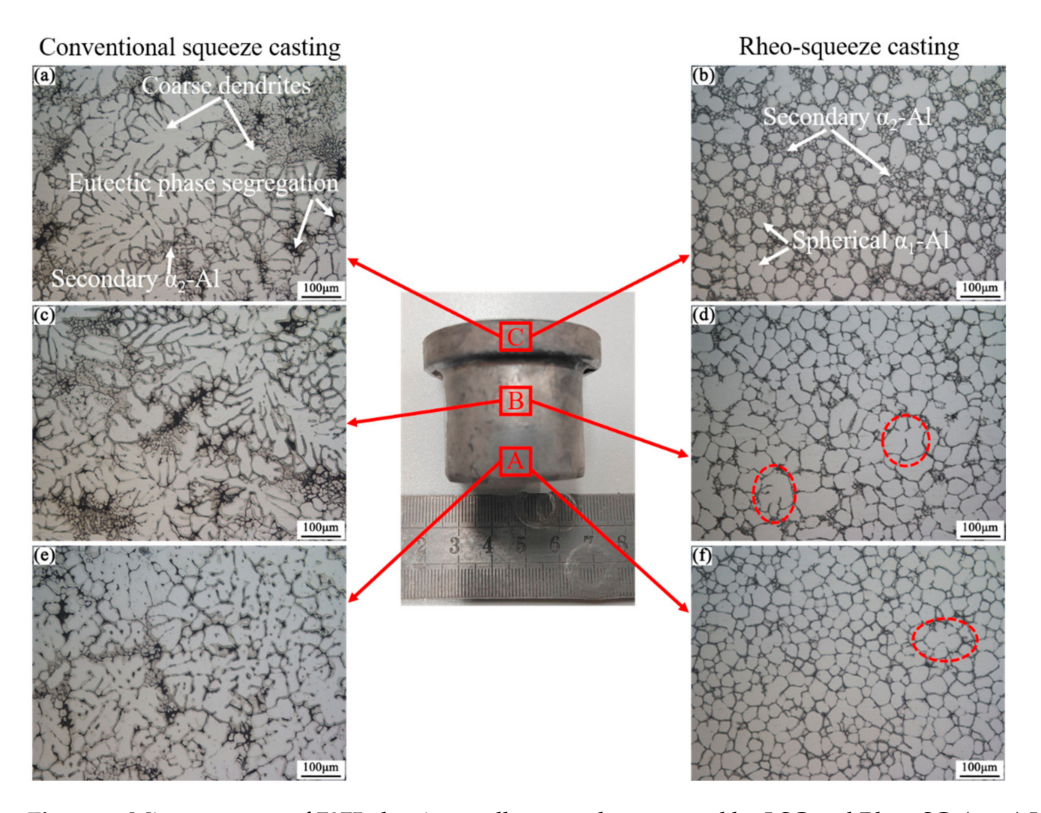


**Figure 8.** Microstructure of 7075 aluminum alloy samples prepared by LSC and Rheo-SC: (**a**,**c**,**e**) LSC; (**b**,**d**,**f**) Rheo-SC.

The Rheo-SC sample's microstructure is made up of subspherical primary  $\alpha_1$ -Al and fine secondary  $\alpha_2$ -Al generated by secondary solidification, according to Figure 8b,d,f. Two solidification processes, the primary solidification in the ECSC and the secondary solidification of the slurry during the filling of the die, resulted in the microstructure of the Rheo-SC sample. The semi-solid slurry created by the ECSC is injected into the barrel, where it fits tightly against the die wall under the pressure of filling, providing a significant subcooling for the nucleation of the remaining liquid phase due to the essential temperature gradient between the die and the slurry. The die wall provides a substrate for its inhomogeneous nucleation so that a significant amount of nucleation will occur. The residual liquid phase in the slurry eventually converges at location C as the injection pressure pushes it in the filling direction, generating a fine secondary solidification subequiaxial grain microstructure with a specific ratio [31]. A semi-solid slurry with a specific fraction solid ( $f_s = 0.3$ ) is used in Rheo-SC. The solid phase of the slurry in the die slows down the cooling, increasing the die's tendency toward equilibrium solidification, lowering the degree of intergranular eutectic phase segregation, and increasing the homogeneity of the distribution, all of which improve the performance [32].

Figure 9 displays the microstructure and related grain size distribution of the LSC and Rheo-SC samples measured by EBSD. Red corresponds to the <001> direction, blue corresponds to the <111> direction, and green corresponds to the <101> direction, with the <X0> direction being parallel to the casting filling direction. The various colors in the picture reflect distinct crystal orientations [33]. Figure 9a,b make it abundantly evident that

Crystals 2023, 13, 1102 10 of 15

the distribution of blue and green is wider than that of red, indicating that the <111> and <101> directions are the principal crystal directions of the casting in the filling direction [34]. In the LSC samples, about 1.82% of the grain size is over 200  $\mu m$ , and 10.21% is over 100  $\mu m$ . In contrast, only 0.86% of grains with a size greater than 100  $\mu m$  and 85% of grains with a size less than 50  $\mu m$  were found in the Rheo-SC samples. In conclusion, compared with the LSC, the size and morphology of the microstructure of the Rheo-SC samples are refined and improved significantly, indicating that the Rheo-SC process can obtain 7075 aluminum alloy castings with a uniform and fine microstructure.

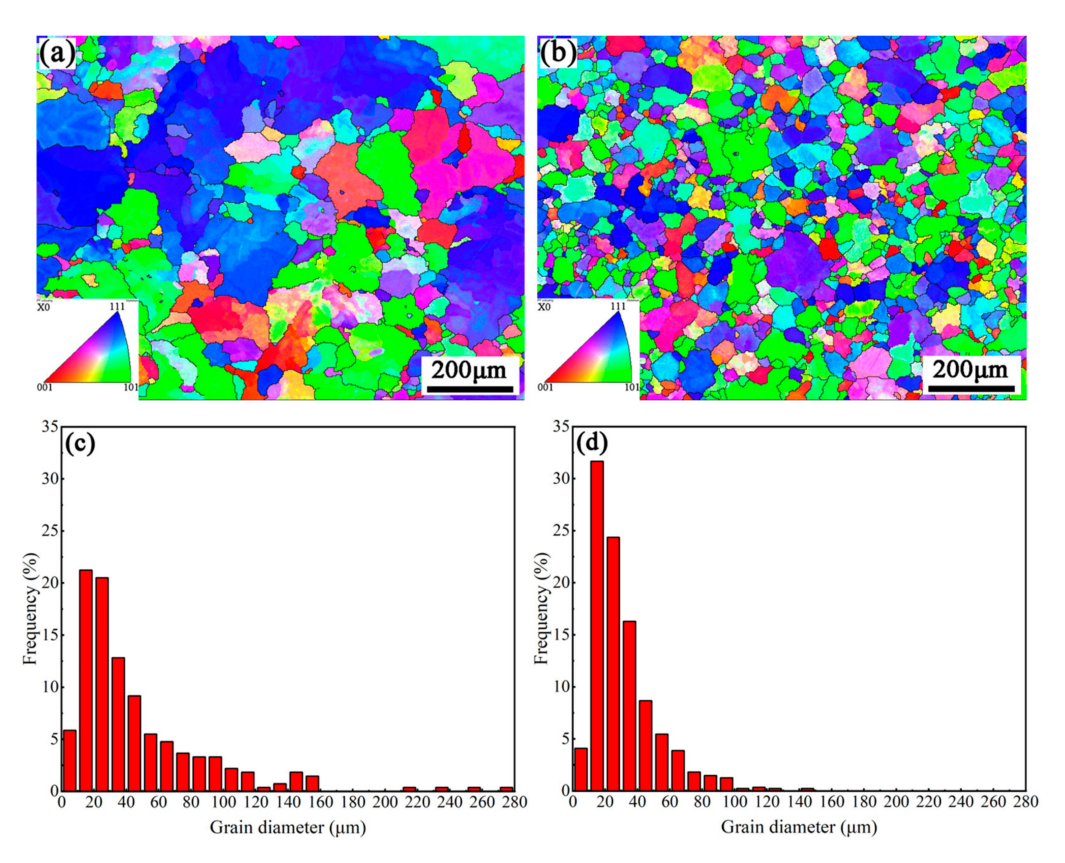


**Figure 9.** EBSD map and relevant grain size distribution: (a) LSC sample; (b) Rheo-SC sample; (c) Relative frequency distribution of grain diameter in LSC samples; (d) Relative frequency distribution of grain diameter in Rheo-SC samples.

Figure 10 shows the EDS of the intergranular second phase of the Rheo-SC samples. The second phase in the 7075 aluminum alloy is mainly composed of Mg(Al, Cu, Zn)<sub>2</sub>, Al<sub>2</sub>Cu, Al<sub>2</sub>CuMg phase, etc. The microstructure of the Rheo-SC sample has a high percentage of Al atoms in the rod-shaped intergranular second phase (as shown at point 1 in Figure 10) and a low percentage of Zn and Mg atoms, with a possible phase composition of MgZn<sub>2</sub>. At point 2, the Cu atomic percentage is higher, and the possible phase composition is Al<sub>2</sub>Cu. The intergranular bright white second phase (position 3) has a high Al to Cu atomic proportion, and the possible phase composition is the Al<sub>2</sub>Cu phase and Al<sub>2</sub>CuMg phase. It is clear to see that during the Rheo-SC process of the 7075 aluminum alloy, Cu elements are prone to intergranular segregation [4,35]. The XRD patterns of the 7075 aluminum alloy samples prepared by LSC and Rheo-SC are shown in Figure 11. It is clear that the samples obtained by LSC or Rheo-SC, which are both composed of the  $\alpha$ -Al, MgZn<sub>2</sub>, and Al<sub>2</sub>Cu phases, have the same phase composition. Lower concentrations are indicated by the MgZn<sub>2</sub> and Al<sub>2</sub>Cu phases' smaller diffraction peaks.

Crystals **2023**, 13, 1102 11 of 15

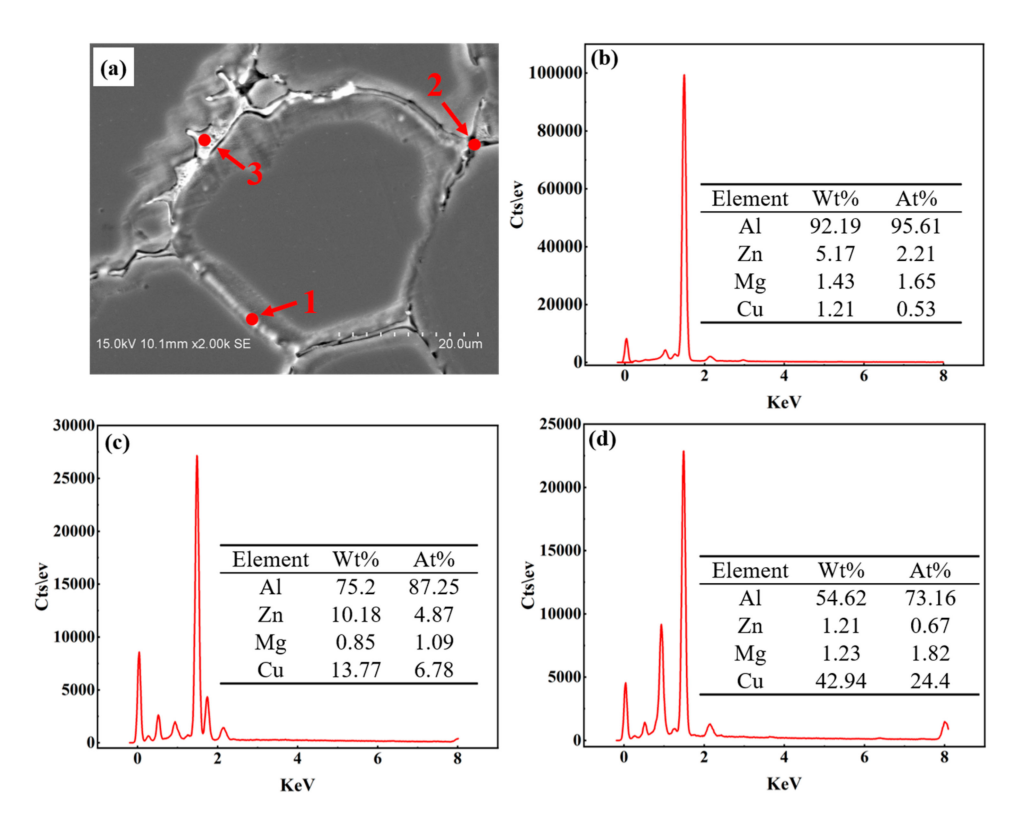


**Figure 10.** EDS analysis of Rheo-SC sample: (a) Sampling points for EDS analyses; (b) point 1; (c) point 2; (d) point 3.

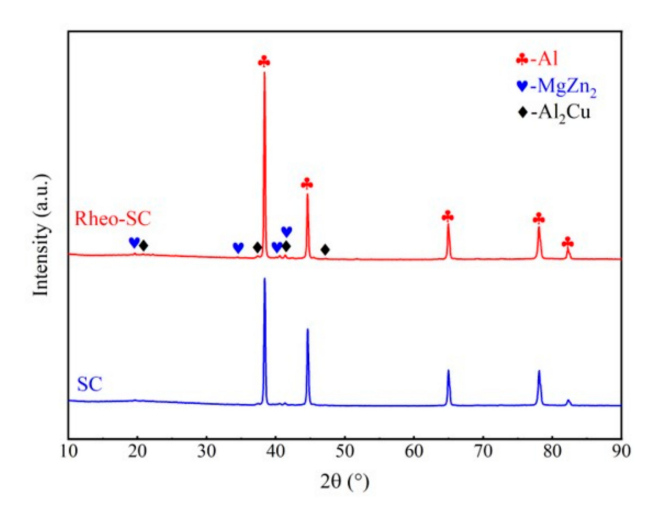


Figure 11. XRD patterns of Rheo-SC and LSC samples.

## 3.3.2. Mechanical Properties and Fracture Morphology

Figure 12 displays the stress–strain curves and tensile properties of the castings made of the 7075 aluminum alloy using various forming techniques. The Rheo-SC samples had ultimate tensile strengths, yield strengths, and elongations that were, respectively, 10%, 10.5%, and 44.4% greater than those of the LSC samples at 238 MPa, 151 MPa, and 5.2%. In the LSC procedure, the high-temperature liquid alloy is injected from the barrel through the sprue into the die cavity. The flow rate of the alloy liquid increases, and air is easily trapped when it passes through the thin wall of the die cavity (positions A and B in Figure 1), causing defects, like pores, to appear in the final solidification microstructure. In addition, the high solidification shrinkage of the liquid alloy can also form shrinkage holes as well as shrinkage loosening in the casting. These defects can easily become the source of crack sprouting during the subsequent tensile experiments, making the specimens fail rapidly

Crystals 2023, 13, 1102 12 of 15

under the tensile stress, and the sample tensile properties perform poorly, especially in terms of elongation. Alternatively, the castings prepared by the LSC process have a coarse dendritic structure, and the coarse dendrites tend to induce stress concentrations, which also affect the tensile properties of the castings.

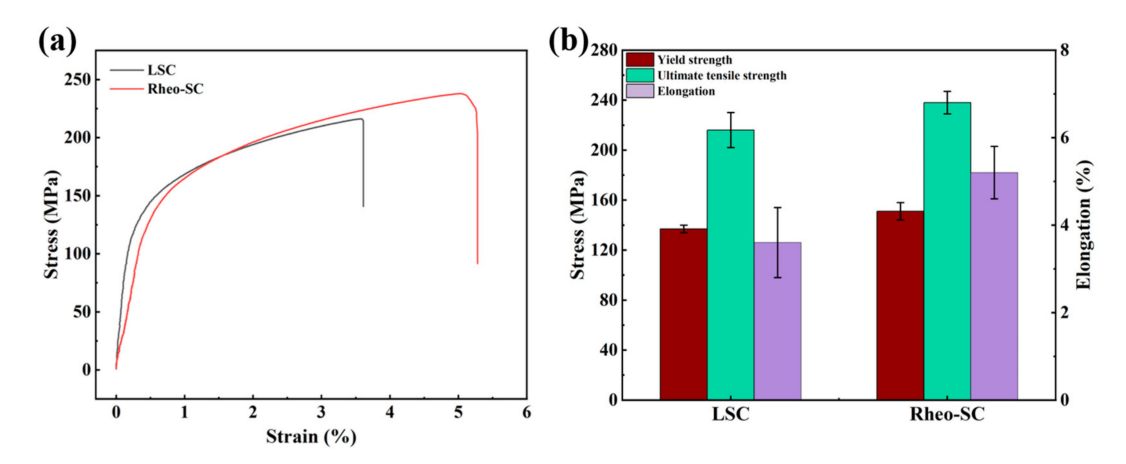


**Figure 12.** (a) Stress–strain curves; (b) Mechanical properties of 7075 alloys in different forming techniques.

In the Rheo-SC process, using a semi-solid slurry with a certain fraction solid ( $f_s=0.3$ ) allows the slurry to flow similarly to laminar flow during the forming process, even in the thin walls of the die. In addition, the semi-solid slurry has less solidification shrinkage, which largely avoids defects, such as porosity and shrinkage, making the castings denser and tighter and improving the tensile properties of the Rheo-SC samples [32]. In addition, the grain refinement of the Rheo-SC samples also contributes to improving their properties. According to the Hall–Petch formula [36]:

$$\sigma_s = \sigma_0 + kd^{-1/2}$$

where  $\sigma_0$  is a constant that represents friction stress, which is approximately 20 Mpa; k is the Hall–Petch coefficient of the Al alloy, which is approximately 40 MPa· $\mu$ m<sup>1/2</sup>; and d is the average grain size. According to the calculation above, the average grain diameter of 34.9  $\mu$ m from numerous metallographic images of Rheo-SC samples taken at various locations equals a contribution value of grain refinement to yield strength of 26.8 MPa. It is clear that reducing the grain size enhances the yield strength. Additionally, the primary  $\alpha_1$ -Al phase is thinned, increasing the number of grain boundaries. This improves the resistance to dislocation movement during the deformation process, creating a strong strengthening impact on the grain boundaries [37,38].

Figure 13 depicts the fracture morphology of the LSC and Rheo-SC samples. On the fracture surface of the LSC samples, casting flaws, including cracks and shrinkage holes, are easily visible. These defects will be the source of crack initiation and accelerate the fracture of samples in the tensile test [39]. As illustrated in Figure 13a,c, the tear ridge and cleavage plane were also visible, but there were no dimples. This suggests that the specimen had a brittle fracture, as indicated by the low 3.6% tensile elongation at ambient temperature. Figure 13b,d depict the fracture morphology of the Rheo-SC samples. It is possible to see several tear ridges and dimples, which are signs of ductile fracture. Further evidence that the fracture type of the Rheo-SC samples was mixed came in the form of a few microcracks and foliating surfaces. This explains why it is impossible to further enhance the tensile properties of the Rheo-SC samples.

Crystals 2023, 13, 1102 13 of 15

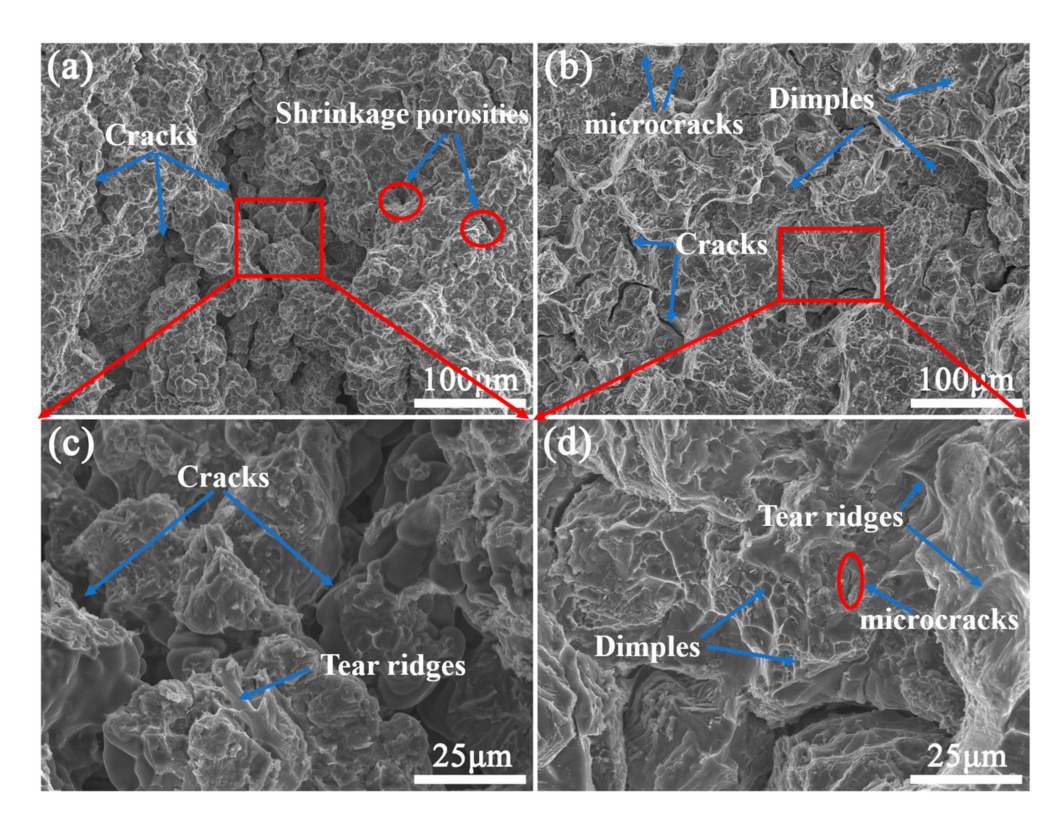


Figure 13. Fracture morphologies: (a,c) LSC sample; (b,d) Rheo-SC sample.

#### 4. Conclusions

In this study, a semi-solid slurry of the 7075 aluminum alloy was prepared using an ECSC technique, and it was subjected to rheological squeeze casting. The microstructure characteristics and mechanical properties of the semi-solid 7075 aluminum alloy were studied. The following are some crucial conclusions that can be drawn:

- (1) A pouring temperature of 670 °C and a rate of cooling water of 200 L/h are the ideal preparation conditions for the semi-solid slurry of the 7075 aluminum alloy, at which point the primary  $\alpha$ -Al's average grain diameter is 35  $\mu$ m, and its shape factor is 0.67.
- (2) Rheo-SC improves the microstructure and the homogeneity of the elemental distribution of 7075 aluminum alloys. EBSD analysis showed that the Rheo-SC samples had a much finer microstructure than the LSC samples. The XRD and EDS analyses indicated that the LSC and Rheo-SC samples consisted mainly of two phases:  $\alpha$ -Al and MgZn<sub>2</sub>.
- (3) The Rheo-SC samples had ultimate tensile strengths, yield strengths, and elongations that were, respectively, 10%, 10.5%, and 44% higher than those of the liquid squeeze cast. These values were 238 MPa, 151 MPa, and 5.2%. Reduced casting flaws and the combined effects of fine grain strengthening and enhanced segregation were primarily responsible for the performance increase.

**Author Contributions:** Z.L., Y.L. and R.Z. designed most of the experiments, Z.L. analyzed the results and wrote this manuscript, Y.L. helped analyze the experiment data and gave some constructive suggestions about how to write this manuscript. Z.L., L.X., Q.W. and L.Z. performed most experiments. Q.J. and B.X. provided financial support. All authors have read and agreed to the published version of the manuscript.

**Funding:** This research was funded by the Yunnan Major Scientific and Technological Projects (Grant NO. 202202AG050011 and NO. 202202AB080011), the Scientific Research Fund of the Education Department of Yunnan Province (No. 2022J0051), the Youth Project of Yunnan Province Basic Research (No. 202301AU070040) and the Young Talent Project of the "Xing dian Talent Support Program" of Yunnan Province in 2022.

Crystals 2023, 13, 1102 14 of 15

## Data Availability Statement: Not applicable.

Acknowledgments: The authors acknowledge funding for this research from the Yunnan Major Scientific and Technological Projects (Grant NO. 202202AG050011 and NO. 202202AB080011), the Scientific Research Fund of the Education Department of Yunnan Province (No. 2022J0051), the Youth Project of Yunnan Province Basic Research (No. 202301AU070040) and the Young Talent Project of the "Xing dian Talent Support Program" of Yunnan Province in 2022. This work is supported by the National-Local Joint Engineering Research Center for Technology of Advanced Metallic Solidification Forming and Equipment, Kunming University of Science and Technology, Kunming, China.

**Conflicts of Interest:** The authors declare no conflict of interest.

#### References

- 1. Dursun, T.; Soutis, C. Recent developments in advanced aircraft aluminium alloys. *Mater. Des.* 2014, 56, 862–871. [CrossRef]
- 2. Hirsch, J. Aluminium in Innovative Light-Weight Car Design. Mater. Trans. 2011, 52, 818–824. [CrossRef]
- 3. Hirsch, J. Recent development in aluminium for automotive applications. Trans. Nonferrous Met. Soc. China 2014, 24, 8. [CrossRef]
- 4. Kim, S.W.; Kim, D.Y.; Kim, W.G.; Woo, K.D. The study on characteristics of heat treatment of the direct squeeze cast 7075 wrought Al alloy. *Mater. Sci. Eng. A-Struct. Mater. Prop. Microstruct. Process.* **2001**, 304, 721–726. [CrossRef]
- 5. Li, C.; Wu, S.S.; Lu, S.L.; Li, J.Y.; Liu, L.F.; Xia, L.Q. Effects of Excessive Zr Content and Ultrasonic Treatment on Microstructure and Mechanical Properties of Al-Zn-Mg-Cu Alloy. *Metals* **2021**, *11*, 13. [CrossRef]
- 6. Li, F.; Peh, W.Y.; Nagarajan, V.; Ho, M.K.; Danno, A.; Chua, B.W.; Tan, M.J. Development of non-flammable high strength AZ91+Ca alloys via liquid forging and extrusion. *Mater. Des.* **2016**, *99*, 37–43. [CrossRef]
- 7. Dasgupta, R.; Xia, Y. Squeeze Casting: Principles and Applications. 2004. Available online: https://www.researchgate.net/publication/295555574\_Squeeze\_casting\_Principles\_and\_applications (accessed on 12 March 2023).
- 8. Li, R.X.; Liu, L.J.; Zhang, L.J.; Sun, J.H.; Shi, Y.J.; Yu, B.Y. Effect of Squeeze Casting on Microstructure and Mechanical Properties of Hypereutectic Al-xSi Alloys. *J. Mater. Sci. Technol.* **2017**, *33*, 404–410. [CrossRef]
- 9. Lu, S.L.; Wu, S.S.; Zhu, Z.M.; An, P.; Mao, Y.W. Effect of semi-solid processing on microstructure and mechanical properties of 5052 aluminum alloy. *Trans. Nonferrous Met. Soc. China* **2010**, *20*, S758–S762. [CrossRef]
- 10. Xiao, G.F.; Jiang, J.F.; Liu, Y.Z.; Wang, Y.; Guo, B.Y. Recrystallization and microstructure evolution of hot extruded 7075 aluminum alloy during semi-solid isothermal treatment. *Mater. Charact.* **2019**, *156*, 13. [CrossRef]
- 11. Zhou, B.; Shuai, L.U.; Kai-Le, X.U.; Chun, X.U.; Wang, Z.Y.; Wang, B.J. Hot cracking tendency test and simulation of 7075 semi-solid aluminium alloy. *Trans. Nonferrous Met. Soc. China* **2020**, *30*, 318–332. [CrossRef]
- 12. Flemings, M.C.; Riek, R.G.; Young, K.P. Rheocasting. Mater. Sci. Eng. 1976, 25, 103–117. [CrossRef]
- 13. Liu, Y.; Gao, M.Q.; Meng, S.C.; Fu, Y.; Li, W.R.; Li, C.H.; Guan, R.G. Solidification behavior and enhanced properties of semi-solid Al-8Si-0.5Fe alloys fabricated by rheo-diecasting. *J. Mater. Res. Technol. JMRT* **2022**, *19*, 3160–3171. [CrossRef]
- 14. Qi, M.F.; Xu, Y.Z.; Li, J.Y.; Kang, Y.L.; Wulabieke, Z. Microstructure refinement and corrosion resistance improvement mechanisms of a novel Al-Si-Fe-Mg-Cu-Zn alloy prepared by ultrasonic vibration-assisted rheological die-casting process. *Corros. Sci.* **2021**, 180, 14. [CrossRef]
- 15. Gao, W.J.; Xing, S.M.; Yan, G.Y.; Zhao, B.W. Effect of oscillation frequency on microstructure of A356 slurry prepared by semi-solid metal forming with flow. *J. Mater. Process. Technol.* **2023**, *311*, 13. [CrossRef]
- 16. Zhou, B.; Qiu, Z.Y.; Chen, K.P.; Xu, C.; Wang, Z.Y. Microstructure, Properties, and Numerical Simulation of Semi-Solid Aluminum Alloy under Planetary Stirring Process. *Materials* **2022**, *15*, 12. [CrossRef]
- 17. Jahanbakhshi, M.; Nourouzi, S.; Naseri, R.; Esfandiari, K. Investigation of Simultaneous Effects of Cooling Slope Casting and Mold Vibration on Mechanical and Microstructural Properties of A356 Aluminum Alloy. *Met. Mater. Int.* **2022**, *28*, 1508–1516. [CrossRef]
- 18. Li, Y.K.; Zhou, R.F.; Li, L.; Xiao, H.; Jiang, Y.H. Microstructures formation, distribution of tin element and properties of CuSn10P1 alloy during controlled by melt cooling. *Mater. Res. Express* **2018**, *5*, 11. [CrossRef]
- 19. Zhang, L.J.; Fan, J.T.; Liu, D.J.; Zhang, M.D.; Yu, P.F.; Jing, Q.; Ma, M.Z.; Liaw, P.K.; Li, G.; Liu, R.P. The microstructural evolution and hardness of the equiatomic CoCrCuFeNi high-entropy alloy in the semi-solid state. *J. Alloys Compd.* **2018**, 745, 75–83. [CrossRef]
- 20. Wang, Y.F.; Zhao, S.D.; Zhang, C.Y. Microstructures and mechanical properties of semi-solid squeeze casting ZL104 connecting rod. *Trans. Nonferrous Met. Soc. China* **2018**, *28*, 235–243. [CrossRef]
- 21. Li, Y.K.; Zhou, R.F.; Li, L.; Xiao, H.; Jiang, Y.H. Microstructure and Properties of Semi-solid ZCuSn10P1 Alloy Processed with an Enclosed Cooling Slope Channel. *Metals* **2018**, *8*, 11. [CrossRef]
- 22. Li, N.Y.; Mao, W.M.; Geng, X.X. Preparation of semi-solid 6061 aluminum alloy slurry by serpentine channel pouring. *Trans. Nonferrous Met. Soc. China* **2022**, 32, 739–749. [CrossRef]
- 23. Das, P.; Samanta, S.K.; Bera, S.; Dutta, P. Microstructure Evolution and Rheological Behavior of Cooling Slope Processed Al-Si-Cu-Fe Alloy Slurry. *Metall. Mater. Trans. A-Phys. Metall. Mater. Sci.* **2016**, 47*A*, 2243–2256. [CrossRef]
- 24. Guan, R.G.; Wang, C.; Shang, J.H.; Xing, Z.H. Semisolid metal forming by novel sloping plate process. *Trans. Nonferrous Met. Soc. China* **2006**, *16*, S1265–S1269. [CrossRef]

Crystals 2023, 13, 1102 15 of 15

25. Li, M.; Li, Y.D.; Zheng, H.Q.; Huang, X.F.; Chen, T.J.; Ma, Y. Solidification behavior of 6061 wrought aluminum alloy during rheo-diecasting process with self-inoculation method. *Trans. Nonferrous Met. Soc. China* **2018**, 28, 879–889. [CrossRef]

- 26. Chapman, B. Heat transfer. Magn. Reson. Mater. Biol. Phys. Med. 1974, 9, 146–151. [CrossRef]
- 27. Liu, Z.Y.; Mao, W.M.; Wan, T.; Cui, G.T.; Wang, W.P. Study on Semi-Solid A380 Aluminum Alloy Slurry Prepared by Water-Cooling Serpentine Channel and Its Rheo-Diecasting. *Met. Mater. Int.* 2021, 27, 2067–2077. [CrossRef]
- 28. Jian, Z.Y.; Chang, F.G.; Yan, W.; Yang, G.C.; Zhou, Y.H. Determination of the critical nucleation frequency in undercooled metal melt. *Prog. Nat. Sci.* **2000**, *10*, 211–217.
- 29. Dong, X.X.; Yang, H.L.; Zhu, X.Z.; Ji, S.X. High strength and ductility aluminium alloy processed by high pressure die casting. *J. Alloys Compd.* **2019**, 773, 86–96. [CrossRef]
- 30. Guan, R.G.; Zhao, Z.Y.; Li, Y.D.; Chen, T.J.; Xu, S.X.; Qi, P.X. Microstructure and properties of squeeze cast A356 alloy processed with a vibrating slope. *J. Mater. Process. Technol.* **2016**, 229, 514–519. [CrossRef]
- 31. Li, Y.K.; Li, L.; Geng, B.Y.; Wang, Q.P.; Zhou, R.F.; Wu, X.; Xiao, H. Microstructure characteristics and strengthening mechanism of semisolid CuSn<sub>10</sub>P<sub>1</sub> alloys. *Mater. Charact.* **2021**, 172, 11. [CrossRef]
- 32. Chang, Z.Y.; Deng, Q.C.; Lan, Q.; Feng, J.; Li, D.Q.; Liu, B.L.; Wu, Y.J.; Peng, L.M.; Ding, W.J. Microstructure and mechanical properties of Mg-Gd-Y-Zn-Zr alloy prepared by rheo-diecasting. *Mater. Sci. Eng. A-Struct. Mater. Prop. Microstruct. Process.* 2022, 848, 10. [CrossRef]
- 33. Wei, Z.Y.; Yuan, M.N.; Shen, X.Q.; Han, F.Z.; Yao, Y.H.; Xin, L.; Yao, L.B. EBSD investigation on the interface microstructure evolution of Ti-Al<sub>3</sub>Ti laminated composites during the preparation process. *Mater. Charact.* **2020**, *165*, 9. [CrossRef]
- 34. Li, N.Y.; Mao, W.M.; Geng, X.X.; Zhang, R.S.; Yan, B.D. Microstructure, segregation and fracture behavior of 6061 aluminum alloy samples formed by semi-solid or traditional high pressure die casting. *Mater. Today Commun.* **2022**, *31*, 16. [CrossRef]
- 35. Mahathaninwong, N.; Plookphol, T.; Wannasin, J.; Wisutmethangoon, S. T6 heat treatment of rheocasting 7075 Al alloy. *Mater. Sci. Eng. A-Struct. Mater. Prop. Microstruct. Process.* **2012**, 532, 91–99. [CrossRef]
- 36. Baek, M.S.; Euh, K.; Lee, K.A. Microstructure, tensile and fatigue properties of high strength Al 7075 alloy manufactured via twin-roll strip casting. *J. Mater. Res. Technol. JMRT* **2020**, *9*, 9941–9950. [CrossRef]
- 37. Wang, X.D.; Zhang, Z.; Wang, Z.B.; Ren, X.C. Excellent tensile property and its mechanism in Al<sub>0.3</sub>CoCrFeNi high-entropy alloy via thermo-mechanical treatment. *J. Alloys Compd.* **2022**, 897, 10. [CrossRef]
- 38. Xiong, Z.F.; Jiang, Y.; Yang, M.; Zhang, Y.; Lei, L. Achieving superior strength and ductility in 7075 aluminum alloy through the design of multi-gradient nanostructure by ultrasonic surface rolling and aging. *J. Alloys Compd.* **2022**, *918*, 14. [CrossRef]
- 39. Qi, M.F.; Kang, Y.L.; Xu, Y.Z.; Wulabieke, Z.; Li, J.Y. A novel rheological high pressure die-casting process for preparing large thin-walled Al-Si-Fe-Mg-Sr alloy with high heat conductivity, high plasticity and medium strength. *Mater. Sci. Eng. A-Struct. Mater. Prop. Microstruct. Process.* 2020, 776, 18. [CrossRef]

**Disclaimer/Publisher's Note:** The statements, opinions and data contained in all publications are solely those of the individual author(s) and contributor(s) and not of MDPI and/or the editor(s). MDPI and/or the editor(s) disclaim responsibility for any injury to people or property resulting from any ideas, methods, instructions or products referred to in the content.